Tandem Tilt-Wing Control Law Design using Hybrid Nonlinear Dynamic Inversion

Daniel Milz* and Marc May† and Gertjan Looye‡
Institute of Flight Systems, German Aerospace Center (DLR), 82234 Weßling, Germany

Nomenclature

t	=	time
$u \in \mathcal{U}$	=	input vector
$x \in \mathcal{X}$	=	state vector
$y \in \mathcal{Y}$	=	output vector
f	=	*internal* dynamics
g	=	input dynamics
h	=	output map
∇	=	nabla operator
$L_f h$	=	Lie derivative of h w.r.t. f
$\boldsymbol{I}$	=	identity matrix
$\boldsymbol{r}$	=	position vector in m
$\boldsymbol{v}$	=	velocity vector in $\frac{\mathrm{m}}{\mathrm{s}}$
$\boldsymbol{\Theta}$	=	Euler angle vector in rad
$\boldsymbol{\omega}$	=	angular rates vector in $\frac{\mathrm{rad}}{\mathrm{s}}$
ϕ	=	roll angle (Euler) in rad
θ	=	pitch angle (Euler) in rad
ψ	=	yaw angle (Euler) in rad
$\mathbb{T}_{AB}$	=	transformation matrix from frame B to A
$\boldsymbol{R}_{\mathrm{y}}$	=	rotation matrix around y-axis
m	=	mass in kg
$\boldsymbol{J}$	=	moment of inertia matrix in $\mathrm{kg\,m^2}$
$\boldsymbol{g}$	=	gravitational acceleration vector in $\frac{\mathrm{m}}{\mathrm{s}^2}$

Presented as publication 2024-4418 at the AIAA AVIATION FORUM AND ASCEND 2024, Las Vegas, NV, July 29 – August 02, 2024
Presented as publication 2025-2698 at the AIAA SCITECH 2025 Forum, Orlando, FL, January 06-10, 2025
*Research Associate, Department of Flight Control and Simulation, daniel.milz@dlr.de, AIAA member, corresponding author
†Research Associate, Department of Flight Control and Simulation, marc.may@dlr.de
‡Head of Department, Department of Control of Aeroelastic Systems, Institute of Aeroelasticity, gertjan.looye@dlr.de

T	=	thrust in N
δ_w	=	tilt-wing angle in rad
δ_e	=	elevon deflection in rad
α	=	angle of attack in rad
β	=	angle of sideslip in rad
$\boldsymbol{f}$	=	force vector in N
$\boldsymbol{m}$	=	moment vector in N m
ρ	=	air density in $\frac{\mathrm{kg}}{\mathrm{m}^3}$
R	=	propeller radius in m
C_T, C_Q	=	propeller thrust and torque coefficient
n	=	propeller rotational velocity in $\frac{1}{\mathrm{s}}$
s_sc	=	slipstream contraction factor
$C_{v\mathrm{t}}$	=	swirl factor
$C_\mathrm{D}, C_\mathrm{Y}, C_\mathrm{L}$	=	Drag, sideforce, lift coefficient
$\boldsymbol{n}_\mathrm{y}$	=	lateral load factor in g
ν	=	virtual control input
$\mathcal{L}^{-1}$	=	Inverse Laplace transformation
L	=	cost function
$\boldsymbol{W}$	=	weighting matrix
τ, τ_0	=	Demanded effect
$\mathcal{G}$	=	controllable subset of g
$\boldsymbol{B}$	=	local input/effect matrix

Subscripts

0	=	reference or expansion point
d	=	demanded value
u	=	input-dependent
x	=	state-dependent
ax	=	axial component
t	=	tangential component
a	=	aerodynamics component
p	=	propeller index
j	=	wing segment index

x, y, z = x-, y-, z-axis

Superscripts

B = body frame

C = control frame

N = North-East-Down frame

W = wing frame

I. Introduction

Transformational vertical take-off and landing (VTOL) aircraft have become pivotal in the context of Advanced Air Mobility. They offer unparalleled flexibility in confined spaces and enable novel operational concepts by seamlessly transitioning between hover and cruise flight. Among the promising configurations are tandem tilt-wing electric VTOLs (eVTOLs), which combine the capability for vertical take-off and landings with an efficient cruise flight, all while using a single propulsion system throughout the entire envelope [1]. However, transformational VTOLs, especially tandem tilt-wings, have intricate mechanics at the tilting mechanism and exhibit complex aerodynamic characteristics, necessitating novel modeling approaches to accurately capture propeller-wing and wing-wing interactions [2, 3]. Moreover, the transition between different flight phases represents a complex and little-studied phenomenon that must be handled in order to allow tilt-wing operations [4]. Nevertheless, multiple endeavors have been conducted on (tandem) tilt-wing configurations, including the CL-84 [5], Airbus A^3 Vahana [6], NASA LA-8 [7], and other mentionable tilt-wing configurations [8–10]. Despite these efforts, controlling those aircraft, particularly during the transition phase, presents a considerable challenge due to the variations in flight dynamics.

Transformational VTOL configurations, such as tilt-wings or tilt-rotors, are inherently non-affine in their input. These characteristics, in combination with complex aerodynamic effects and interactions, create a distinctive control problem, making the flight control design a challenging task. Furthermore, VTOL aircraft can have more degrees of freedom that classical fixed-wing aircraft by for instance allowing to control the thrust vector direction. VTOL aircraft, especially in conjunction with distributed electric propulsion, are often overactuated systems that require a suitable control allocation scheme. Common requirements for the flight control laws are that there are neither (explicit) switching nor predefined maneuvers involved between different flight modes, an intuitive and clean interface to the pilot that allows easy flying in the whole envelope, and an efficient use of all available control effectors [11, 12].

Widespread methods for controlling these vehicles are among others [13], especially gain-scheduling of PID control laws [14], robust H_∞ control laws [15], or optimal LQR control laws [16–18]. The commonality of these linear methods is that they are only partly suitable for these complex nonlinear dynamics, and inherently require scheduling techniques to ensure satisfactory performance over the different flight regimes. This increases the design effort, since the synthesis

must be performed for multiple flight conditions. Additionally, the conflation of the different designs should ensure a smooth transition between them, through appropriate scheduling or parameterization schemes over the whole flight envelope. Alternative approaches employ adaptive control techniques [19, 20] and dynamic inversion-based control laws [8, 11, 21–26]. The latter is the most popular method currently applied, as it provides an inherent solution to the aforementioned requirements while simultaneously providing physical interpretation, (global) decoupling of the dynamics, and a modular and reusable flight controller design [24]. Those approaches, however, assume a control-affine system or schedule the transformational input variable (e.g., the tilt-angle) feed forward.

This work builds on previous research [21, 27] on the tandem tilt-wing configuration depicted in Figure 1 and described in [28]. We extend previous work by introducing a *unified* control approach for the entire envelope, using hybrid nonlinear dynamic inversion (hybrid NDI) integrated with a control allocation scheme that handles all control axes collectively. Hybrid NDI [29, 30] is a promising method for flight control because it allows a trade-off between model-based and sensory, or sensor-based, NDI. While increasing the robustness to model uncertainties, hybrid NDI dampens the aggressiveness of sensory NDI while providing an intuitive control allocation task based on absolute commands. This allows for full envelope control of transformational VTOLs. In contrast to similar approaches [8, 11, 22–26], this work integrates the inversion of the angular rate and velocity dynamics to generate thrust, control surface, and tilt angle commands in a unified manner. As all axes are handled in the same control allocation task, it allows for an optimal allocation and better handling of the vehicle during transition maneuvers. Furthermore, the tilt angle is controlled via feedback, which enables "pitch-supported tilting" to mitigate tilt-actuator limitations during transition maneuvers. Using the proposed approach, we can select the controlled variables and control structure holistically for the entire envelope, leading to a *unified inversion* [21]. The presented methods are designed for the broader class of transformational VTOLs, and the proposed control approach is derived generically. However, this work demonstrates the application to a particular tandem tilt-wing eVTOL configuration (shown in Fig. 1).

This paper is structured as follows: Section II describes the tandem tilt-wing aircraft and the flight dynamics model. Section III details the proposed flight control concept on the generic model. In Section III.C, we apply this concept to the flight control law design of the tandem tilt-wing model from [28] and implement the attitude and flight path control loops. The controller is tested by means of different transition maneuvers [4], which are presented and discussed in Section IV. Finally, Section V concludes the study.

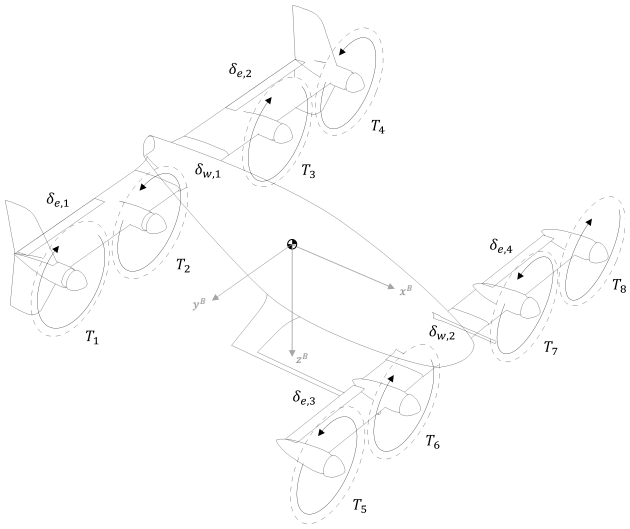

Fig. 1 3D sketch of the tandem tilt-wing configuration with annotated input variables.

II. Flight Dynamics Model

We assume a nonlinear non-affine system of the form

$$\begin{cases} \dot{x} = f(x) + g(x,u) & \text{(1a)} \\ y = h(x) & \text{(1b)} \end{cases}$$

where f, g, and h are smooth vector fields.

Although most fixed-wing aircraft and the common derivation for NDI-based control laws are based on a control-affine nonlinear system, transformational VTOLs and particularly tilt-wings are inherently non-affine. Based on this, we will derive a generic nonlinear, non-affine 6-DoF rigid-body flight dynamics model, as used for instance for a tandem tilt-wing eVTOL.

The nonlinear state-space representation of the tandem tilt-wing eVTOL can be described by

$$\dot{\boldsymbol{r}}^N = \mathbb{T}_{\mathrm{NB}}(\boldsymbol{\Theta})\, \boldsymbol{v}^B \tag{2a}$$

$$\dot{\boldsymbol{\Theta}} = \mathbb{T}_{\Theta\mathrm{B}}(\boldsymbol{\Theta})\, \boldsymbol{\omega}^B \tag{2b}$$

$$\dot{\boldsymbol{v}}^B = -\boldsymbol{\omega}^B \times \boldsymbol{v}^B + \boldsymbol{g}^B + \frac{1}{m}\boldsymbol{f}^B(x,u) \tag{2c}$$

$$\underbrace{\dot{\boldsymbol{\omega}}^B}_{\dot{x}} = \underbrace{\boldsymbol{J}^{-1}\left(-\boldsymbol{\omega}^B \times \boldsymbol{J}\boldsymbol{\omega}^B\right)}_{f(x)} + \underbrace{\boldsymbol{J}^{-1}\boldsymbol{m}^B(x,u)}_{g(x,u)} \tag{2d}$$

with the state vector $x = \left[\boldsymbol{r}^N,\ \boldsymbol{\Theta},\ \boldsymbol{v}^B,\ \boldsymbol{\omega}^B\right]^T$ and the input vector $u = \left[T_{1\ldots8}, \delta_{\mathrm{w},1\ldots2}, \delta_{\mathrm{e},1\ldots4}\right]^T$ annotated in Fig. 1. Furthermore, $\mathbb{T}_{\mathrm{NB}}$ and $\mathbb{T}_{\Theta\mathrm{B}}$ denote the transformation matrix from the body frame to the earth frame and for the

Euler derivatives, respectively.Transformational VTOLs are also described by their current *form* represented by the transformation state $\boldsymbol{\sigma}$. For instance, the current tilt angle describes the transformation state for tilt-wing VTOLs. For simplicity, we assume $\boldsymbol{\sigma} = u_\sigma$ and u_σ being subject to actuator dynamics.

A. Tandem Tilt-Wing Flight Dynamics

The flight dynamics model of the tandem tilt-wing aircraft (Fig. 1) is introduced in [28], uses a strip-theory model with empirical corrections, and contains a variable weight and balance model and motor and propeller models. It is governed by the nonlinear 6-DoF equations Eq. (2). The configuration is characterized by 14 control inputs and distinguishes itself from other configurations by having eight electrically driven propellers T_i, two independent tandem tilt-wings $\delta_{\mathrm{w},i}$, and four (one per half-wing) elevons $\delta_{\mathrm{e},i}$. They allow direct control over $\boldsymbol{m}^B$, and the x- and z-component of $\boldsymbol{f}^B$. The wings have vertical and horizontal displacement in order to minimize possible interactions, especially propeller-propeller interactions. The elevons lie in the wetted surface area of both propellers, which leads to an additional slipstream-interaction effect. Finally, the propeller rotation directions are chosen to allow a complete moment cancellation in nominal flight and to allow yaw maneuvers during hover flight using differential thrust.

However, a simpler model is used for control design and implementation, allowing an efficient computation of the flight dynamics and quick estimation of the current B-matrix (see Eq. (14b)) online. The reduced model uses the same nonlinear 6-DoF equations of motion but covers the aerodynamic effects with a simplified *minimal strip model* following the formulation in [2, 28]. Each half wing is only divided into three *strips*: The first strip is located mainly in the slipstream of the inner half of the inner propeller, the second one in the slipstream of the outer half of the inner propeller, and the last is primarily in the slipstream of the inner half of the outer propeller. A more detailed description of this reduced strip-theory model can be found in [4]. This approach effectively accounts for the dominant effects of the tilt-wing dynamics, mainly the nonlinear and distributed aerodynamics, including propeller-slipstream effects. However, effects such as (smooth) lift distribution, distributed propeller swirl, or interactions between the tandem wings are neglected. Yet, the quick comparison between both models shown in [4, 27] suggests that the longitudinal forces and moments match sufficiently well for control design.

The system Eq. (2) consists of the flight mechanical equations and depends on the applied forces and moments. Those mainly consist of the propulsion forces and moments and the aerodynamic forces and moments, which are described subsequently.

The propulsive forces and moments are approximated by a simple propeller model solely depending on the current rotational velocity n in $1/\mathrm{s}$:

$$\boldsymbol{f}^B_{\mathrm{p},x} = \rho\,(2R)^4\,C_T\,n^2 \tag{3a}$$

$$\boldsymbol{m}^B_{\mathrm{p},x} = \rho\,(2R)^5\,C_Q\,n^2 \tag{3b}$$

with the the propeller radius $R = 0.75\,\mathrm{m}$, the thrust constant $C_T \approx 0.133$ and the torque constant $C_Q \approx 0.0345$.

The aerodynamic effects are approximated through a strip theory approach as described in detail in [28]. The main effect is assumed to be the propeller slipstream induced axial velocity in the wing frame v_{ax}^W, which adds up to the free flow velocity in the wing frame $\boldsymbol{v}^W$. The induced velocity from the propeller p can then be approximated as

$$v_{\mathrm{ax},p}^W(v^B, \delta_{\mathrm{w},p}, T_p) = \frac{s_{\mathrm{sc}}}{2}\left(-\left(\boldsymbol{v}^B\right)_{\mathrm{x},p}^W + \sqrt{\left(\left(\boldsymbol{v}^B\right)_{\mathrm{x},p}^W\right)^2 + \frac{2\,T_p}{\rho\pi R^2}}\right) \tag{4}$$

with the mean slipstream contraction factor $s_{\mathrm{sc}} \approx 1$ [31] and the free flow velocity acting on the current propeller p

$$\left(\boldsymbol{v}^B\right)_p^W = \boldsymbol{R}_{\mathrm{y}}\left(\delta_{\mathrm{w},p}\right)\left(\boldsymbol{v}^B + \boldsymbol{\omega}^B \times \boldsymbol{r}_p^B\right) \tag{5}$$

with the position of the propeller in the body frame $\boldsymbol{r}_p^B$. The swirl induces an additional tangential velocity on the wing segments behind the propeller and can be approximated as derived in [31] as

$$v_{\mathrm{t},p}^W = \pm C_{v\mathrm{t}}\sqrt{T_p} \tag{6}$$

with the swirl factor $C_{v\mathrm{t}} \approx 0.03$ [31] and the direction depending on the propeller rotation direction as shown in Fig. 1. The total velocity vector on each wing segment j in the wing frame is then given as

$$\boldsymbol{v}_j^W = \left(\boldsymbol{v}^B\right)_j^W + \begin{bmatrix} v_{\mathrm{ax},p}^W & 0 & v_{\mathrm{t},p}^W \end{bmatrix}^T \tag{7}$$

where the mapping between the propellers and wing segments is in such a way that the four outer wing segments are completely wetted by the outer propellers, and the inner segments each by one half the propeller.

The aerodynamic forces and moments are stated using aerodynamic coefficient functions of the angle of attack and control surface deflection, as described in [31]. The three dimensional distribution of those induces the roll and yaw moments of the overall aircraft. Each segment j generates a lift and drag force as well as a pitch moment. The main contributions to the side force are the fuselage, the inverted V, and the wingtips. Furthermore, the fuselage exhibits a lift and drag force, too, which is assumed to only depend on the free flow.

The total aerodynamic forces $\boldsymbol{f}_{\mathrm{a}}^B$ and moments $\boldsymbol{m}_{\mathrm{a}}^B$ resolved in the body frame are approximated by the aerodynamic

effects, forces and moments of the body B and the wing (W) segments $1 \leq j \leq 12$

$$\boldsymbol{f}_{\mathrm{a}}^{B} = \sum_{j} \underbrace{\frac{1}{2}\rho \left\|\boldsymbol{v}_{j}^{W}\right\|_{2}^{2} \boldsymbol{R}_{\mathrm{y}}\left(\alpha_{j}^{W} - \delta_{\mathrm{w},j}\right) \begin{bmatrix} -C_{\mathrm{D}}^{W}\left(\alpha_{j}^{W}, \delta_{\mathrm{e},j}\right) \\ 0 \\ -C_{\mathrm{L}}^{W}\left(\alpha_{j}^{W}, \delta_{\mathrm{e},j}\right) \end{bmatrix}}_{\boldsymbol{f}_{j}^{B}} + \frac{1}{2}\rho \left\|\boldsymbol{v}^{B}\right\|_{2}^{2} \begin{bmatrix} -C_{\mathrm{D}}^{B}\left(\alpha^{B}\right) \\ C_{\mathrm{Y}}^{B}\left(\beta^{B}\right) \\ -C_{\mathrm{L}}^{B}\left(\alpha^{B}\right) \end{bmatrix} \tag{8a}$$

$$\boldsymbol{m}_{\mathrm{a}}^{B} = \sum_{j} \frac{1}{2}\rho \left\|\boldsymbol{v}_{j}^{W}\right\|_{2}^{2} \boldsymbol{R}_{\mathrm{y}}\left(\alpha_{j}^{W} - \delta_{\mathrm{w},j}\right) \begin{bmatrix} 0 \\ C_{\mathrm{m}}^{W}\left(\alpha_{j}^{W}, \delta_{\mathrm{e},j}\right) \\ 0 \end{bmatrix} + \boldsymbol{r}_{j}^{B} \times \boldsymbol{f}_{j}^{B} \tag{8b}$$

with the wing segment position in the body frame $\boldsymbol{r}_{j}^{B}$ and the angle of attack α and sidelip β being calculated from the corresponding velocity vector.

III. Flight Control Design

The overall control architecture is shown in Fig. 2. Note the combination of dynamic inversion and control allocation, as well as the parallel separation of attitude and flight path controllers. However, coordination between the attitude and flight path control loops is crucial. Furthermore, the switch between pilot inputs and autoflight functions is a handy addition for developing and researching handling qualities and pilot interactions, as well as (partly) autonomous flights.

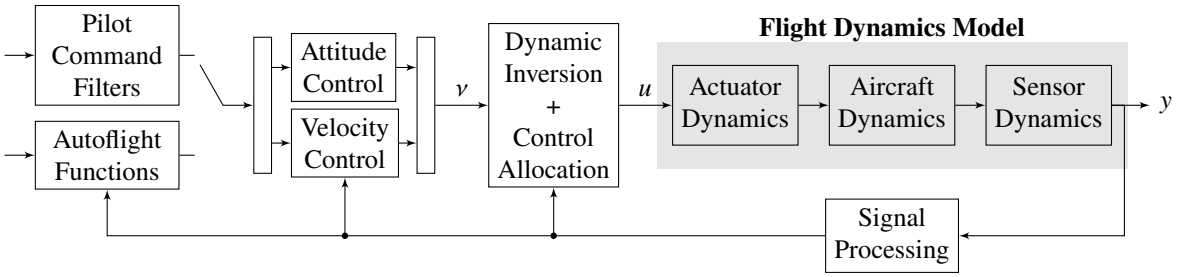

Fig. 2 Proposed control architecture for dynamic inversion-based tandem tilt-wing control.

This approach employs a hybrid NDI control law combined with an optimization-based control allocation, which inverts the rotational and translational dynamics in one. In contrast, most previous works have employed a control concept with separated rotational inversion and translational control [8, 14, 25, 32]. However, combining both makes it possible to leverage specific vehicle characteristics. On the downside, this approach drastically increases the complexity of the inversion. However, by synthesizing this block, all control functions built upon it can be realized relatively independently of the vehicle structure. This allows for a modular control design, in which individual control functions

can be developed and readily integrated into the overall system. The flight control law is initially abstractly derived, yielding the implicit equation Eq. (12) for the non-affine hybrid NDI law. This implicit equation is, however, solved using the control allocation, resulting in the final implementable law shown in Eq. (15).

A. Hybrid Nonlinear Dynamic Inversion

Hybrid NDI combines both model-based and sensory NDI through a complementary filter. In order to arrive at the final hybrid NDI law, model-based and sensory NDI are derived first. The derivation of the control laws is done using Eq. (1) and assuming a relative degree of one, although the control law can be derived for higher relative degrees similarly.

Model-based NDI is *classical* NDI or Feedback Linearization. For a non-affine system, the NDI law relating the required input u to realize the virtual control input ν can be described via the implicit equation

$$\left(L_g h\right)(\hat{x}, u) = \nu - \left(L_f h\right)(\hat{x}) \tag{9}$$

where $\hat{}$ denotes estimated or measured quantities, $\left(L_f h\right)(x)$ the Lie-derivative of h with respect to f, and $\nu \equiv \dot{y}$ being the virtual control input representing the commanded output derivatives.

Sensory NDI [21] or sensor-based NDI uses a similar approach to incremental NDI [33] by substituting the term $L_f h(\hat{x})$ in Eq. (9) with sensor measurements, i.e., $L_f h(\hat{x}) \approx \hat{\dot{y}} - (L_g h)(\hat{x}, \hat{u})$. Thus, the control law can be written implicitly as

$$(L_g h)(\hat{x}, u) = \nu - \hat{\dot{y}} + (L_g h)(\hat{x}, \hat{u}) \tag{10}$$

While the method does not depend on f, it is exposed to the measurements $\hat{\dot{y}}$ and $\hat{u}$, which must be available in sufficient quality and synchronized. Furthermore, both measurements have a direct link to the commanded control input u through the control law. These issues are well known and addressed in, e.g., [29, 34–36].

Hybrid NDI addresses the issues of sensory and model-based NDI by using both methods complementary, i.e., sensory NDI for lower frequencies and model-based NDI for higher frequencies [29, 37]. The hybrid NDI control law for a relative degree of 1 is given by [30]

$$\left(L_g h\right)(\hat{x}, u) = \nu - \mathcal{F}_{\text{compl}} \begin{cases} (L_f h)(\hat{x}), & \text{high-pass} \\ \hat{\dot{y}} - (L_g h)(\hat{x}, \hat{u}), & \text{low-pass} \end{cases} \tag{11}$$

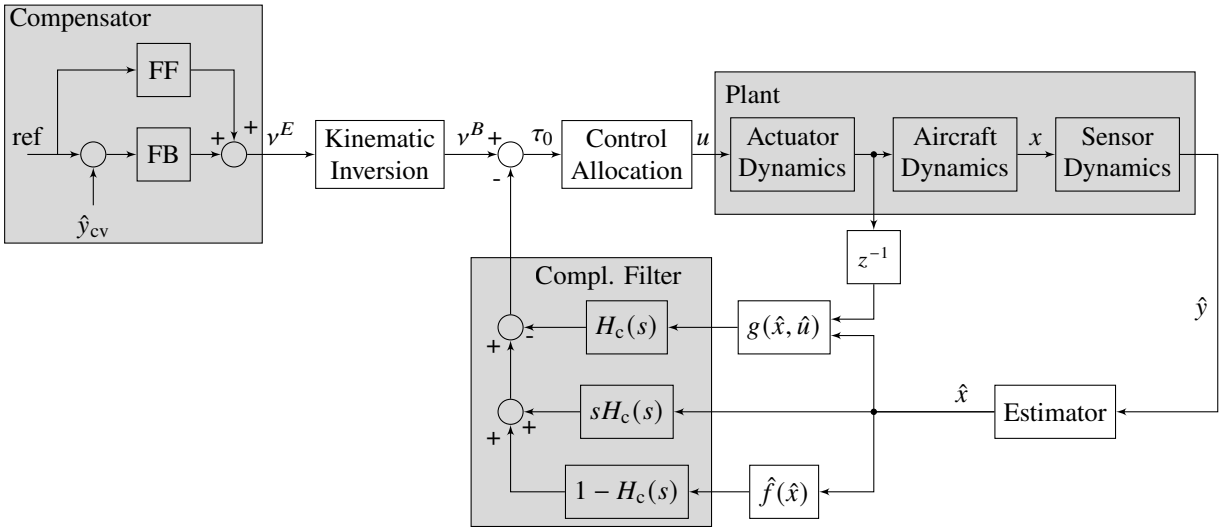

Fig. 3 Schematics of hybrid NDI control structure with an integrated complementary filter [30] and outer loop feed forward (FF) and feedback (FB) compensators.

where the function $\mathcal{F}_{\text{compl}}$ represents a complementary filter. Assuming full-state observation, i.e., $h(x) = x$, and a linear low-pass complementary filter function $H_c(s)$, Eq. (11) can be simplified to

$$g(\hat{x}, u) = \underbrace{\nu - \mathcal{L}^{-1}\left\{H_c(s)\right\} * \left(\hat{\hat{x}} - g(\hat{x},\hat{u})\right) - \mathcal{L}^{-1}\left\{(1 - H_c(s))\right\} * f(\hat{x})}_{\tau_0} \tag{12}$$

using the inverse Laplace transformation $\mathcal{L}^{-1}$ and the convolution operator $*$. Figure 3 shows the implementation schematically. The complementary filter is implemented in an integrated way with shared states between $H_c(s)$, $sH_c(s)$, and $(1 - H_c(s))$ as shown, e.g., in [29, 30, 37]. Furthermore, by using this complementary filter implementation, we can circumvent the differentiation of the estimated states or the need for measured accelerations by "pulling $\hat{\hat{x}}$ through the integrator", resulting in a simpler and potentially more robust implementation of the control law.

The general implicit equation Eq. (12) needs to be solved for the input u either analytically, by nonlinear equation solvers or look-up tables, or by using local approximations. In the scope of this work, the latter is done by employing the Taylor series expansion around an arbitrary expansion point u_0 in combination with a control-allocation scheme. This approximation is similar to the incremental NDI law [33, 38] if used solely with the sensory NDI law and using the currently measured control command as the expansion point, i.e., $u_0 = \hat{u}$. A more detailed discussion on this topic is given in [30].

B. Control Allocation with Dynamic Inversion Constraint

Control allocation is required to solve the dynamic inversion problem for systems where $\dim u > \dim \nu$. This includes the tandem tilt-wing configuration. Therefore, a minimization problem is introduced with an arbitrary scalar

cost function $L : \mathcal{X} \times \mathcal{U} \mapsto \mathbb{R}$ and the *dynamic inversion constraint* as

$$\min_{u \in \mathcal{U}} L(\hat{x}, u) \quad \text{s.t. } \mathcal{G}(\hat{x}, u) = \tau_0 \tag{13}$$

where $\mathcal{G}$ is the controllable subset of g and τ_0 represents the right hand side of Eq. (12) (cf. Section III.C). Typically, L is a convex function of the deviation of the control input $\boldsymbol{u}$ from a reference control input, typically an energy-optimal setting.

In order to arrive at an explicit solution to the above problem, we assume that the system can locally be approximated as control-affine by using series expansions. We utilize the Taylor series expansion in u to the second order for $L(x, u)$ and the first order for $\mathcal{G}(x, u)$ around an arbitrary expansion point u_0. Assuming sufficiently small residuals, we arrive at the surrogate problem of Eq. (13) in the form of a quadratic programming problem subject to linear constraints:

$$\min_{u \in \mathcal{U}} \nabla_u L(\hat{x}, u_0)\,(u - u_0) + \frac{1}{2}\,(u - u_0)^T\,\nabla_{uu} L(\hat{x}, u_0)\,(u - u_0) \tag{14a}$$

$$\text{s.t. } \underbrace{\nabla_u \mathcal{G}(\hat{x}, u_0)}_{B}\, u = \underbrace{\tau_0 - \mathcal{G}(\hat{x}, u_0) + \nabla_u \mathcal{G}(\hat{x}, u_0) u_0}_{\tau} \tag{14b}$$

with the local effect or input matrix B and the demanded effect τ. In contrast to similar approaches, the expansion point u_0 does not need to be the current (measured) input $\hat{u}$. This way, multiple iterations can be used to approximate the solution u. The problem Eq. (14) can be solved explicitly as [27]

$$u = B^+ \tau + \left(I - B^+ B\right) \left(u_0 - \nabla_{uu} L(\hat{x}, u_0)^{-1}\,\nabla_u L(\hat{x}, u_0)\right) \tag{15}$$

with the weighted pseudo-inverse $B^+ = \nabla_{uu} L(\hat{x}, u_0)^{-1} B^T \left(B\,\nabla_{uu} L(\hat{x}, u_0)^{-1}\,B^T\right)$. This allows for a locally optimal control allocation fulfilling the hybrid NDI law. The latter part of Eq. (15) is a term that lies in the null space of B and thus allows a change of u without affecting the effect $B \cdot u$. This can be proven through the identity $B \cdot (I - B^+ B) = 0$.

A detailed discussion about the design of an optimization-based control allocation in combination with dynamic inversion for transformational eVTOLs is given in [8, 27] and for other configurations in [39, 40].

C. Tandem Tilt-Wing Flight Control Design

The proposed control approach is applicable to (many) transformational VTOLs. However, further discussion is required for the application to the tandem tilt-wing. The main one is the selection of controlled variables [41]. As indicated by the flight dynamic equations Eq. (2) and according to common practice, the angular velocities in the body frame $\boldsymbol{\omega}^B$ are selected for the rotational dynamics, since there exists a direct and physical relation to the applied controlling moments and control effectors. The attitude represented by Euler angles can be controlled by using the

kinematic relation between the angular rates and the Euler angle rates. In the context of multi-phase flight, selecting the velocities in the control frame $\boldsymbol{v}^C$ is an elegant solution to represent the translational dynamics, as motivated, for instance, in [11]. The control frame corresponds to the NED frame rotated by the vehicle's heading, i.e., horizontal to the earth surface and aligned with the heading.

However, the inversion itself is designed on the body frame equations. Kinematic relations are used to translate the commanded accelerations from the control into the body frame:

$$\dot{\boldsymbol{\omega}}^B = \dot{\mathbb{T}}_{\Theta B}^T \dot{\boldsymbol{\Theta}} + \mathbb{T}_{\Theta B}^T \ddot{\boldsymbol{\Theta}} \tag{16a}$$

$$\dot{\boldsymbol{v}}^B = \dot{\mathbb{T}}_{CB}^T \boldsymbol{v}^C + \mathbb{T}_{CB}^T \dot{\boldsymbol{v}}^C \tag{16b}$$

with the transformation matrix from the body to control frame $\mathbb{T}_{CB}$.

For the tandem tilt-wing eVTOL control design, we invert the dynamics of $\boldsymbol{\omega}^B$, $\boldsymbol{v}_{\mathrm{x}}^B$, and $\boldsymbol{v}_{\mathrm{z}}^B$ from Eq. (2d) and (2c), which have a relative degree of 1. Note that we cannot control $\boldsymbol{v}_{\mathrm{y}}^B$ directly in this aircraft configuration. We can apply Eq. (12) and (13) using

$$\mathcal{G}(\hat{x}, u) := \begin{bmatrix} \frac{1}{m} & 0 & 0 & \mathbf{0} \\ 0 & 0 & \frac{1}{m} & \mathbf{0} \\ \mathbf{0} & \mathbf{0} & \mathbf{0} & \boldsymbol{J}^{-1} \end{bmatrix} \begin{bmatrix} \boldsymbol{f}^B(\hat{x}, u) \\ \boldsymbol{m}^B(\hat{x}, u) \end{bmatrix} \tag{17}$$

Note that this formulation is in the form of a nonlinear constraint, and the control command u is defined implicitly. The implicit function theorem states that Eq. (17) can be solved for u in a neighborhood of a given u_0 and $x_0 = \hat{x}$, if $\nabla_u \mathcal{G}(x, u)\big|_{\substack{x=\hat{x} \\ u=u_0}}$ has rank 5 [42, Theorem 2-13].

D. Flight Control Law Implementation

The flight control laws are implemented following the previous section. The cost function for the allocation is defined as the convex function

$$L(x, u) = \frac{1}{2} (u - u^*)^T \boldsymbol{W} (u - u^*) \tag{18}$$

with the optimal control input u^* and the weight matrix $\boldsymbol{W}$ which is chosen according to common practice as the inverse of the maximum rates of the normalized input, i.e., the control input is normalized according to its range and then weighted according to its maximum rates:

$$W_{ii} = \frac{1}{\bar{\dot{u}}_i - \underline{\dot{u}}_i} \frac{1}{(\bar{u}_i - \underline{u}_i)^2}, \qquad W_{ij} = 0 \;\; \forall\, i \neq j$$

with upper bound $\bar{u}$ and lower bound $\underline{u}$ and for the control input vector u. The optimal control input u^* is constant at each time step and represents an estimated and desired optimal allocation that may be determined by predefined trajectories. In this work, u^* is set close to the current allocation, thereby ensuring smooth commands, though the propeller speeds are slightly reduced to obtain a lower-power allocation. This leads to the following Taylor series expansion around an arbitrary $u_0 \in \mathcal{U}$ used as the final control-allocation and inversion law Eq. (15):

$$L(x,u) = \underbrace{\frac{1}{2}\left(u_0 - u^*\right)^T \boldsymbol{W} \left(u_0 - u^*\right)}_{L(x,u_0)} + \underbrace{\left(u_0 - u^*\right)^T \boldsymbol{W}}_{\nabla_u L(x,u_0)} \left(u - u_0\right) + \frac{1}{2}\left(u - u_0\right)^T \underbrace{\boldsymbol{W}}_{\nabla_{uu} L(x,\,u_0)} \left(u - u_0\right) \tag{19}$$

The virtual control input vector ν is 5-dimensional and consists of rotational and translational acceleration commands. The angular accelerations $\dot{\boldsymbol{\omega}}^B$ realize the Euler angle accelerations $\ddot{\phi}$, $\ddot{\theta}$, and $\ddot{\psi}$. The commanded yaw acceleration $\ddot{\psi}$ for the kinematic inversion is chosen to be the current (measured) one. However, the finally propagated acceleration in body frame $\dot{r}$ is externally overwritten by either the yaw or sideslip controller [21]. The translational accelerations in horizontal and vertical directions $\dot{\boldsymbol{v}}_{\mathrm{x}}^B$ and $\dot{\boldsymbol{v}}_{\mathrm{z}}^B$ are calculated from the accelerations in the control frame $\dot{\boldsymbol{v}}_{\mathrm{x}}^C$ and $\dot{\boldsymbol{v}}_{\mathrm{z}}^C$. The virtual control input vector prior to the kinematic conversion is thus denoted as $\nu = \left[\nu_\phi,\ \nu_\theta,\ \nu_r,\ \nu_{\dot{v}_{\mathrm{x}}^C},\ \nu_{\dot{v}_{\mathrm{z}}^C}\right]^T$ and calculated through the linear compensators: the attitude and velocity controllers.

E. Attitude Control

The attitude controller is equivalent to the one described in [21] and tracks the Euler angle attitude $\boldsymbol{\Theta}$ through the dynamic inversion with the virtual control inputs $\nu_\omega = \left[\nu_\phi,\ \nu_\theta,\ \nu_r\right]^T$. Those are derived from the control law

$$\nu_\phi = \left(K_{\mathrm{p},\phi} + \frac{K_{\mathrm{i},\phi}}{s}\right)\left(\phi_{\mathrm{d}} - \hat{\phi}\right) + K_{\mathrm{d},\phi}\left(\dot{\phi}_{\mathrm{d}} - \hat{\dot{\phi}}\right) + \ddot{\phi}_{\mathrm{d}} \tag{20a}$$

$$\nu_\theta = \left(K_{\mathrm{p},\theta} + \frac{K_{\mathrm{i},\theta}}{s}\right)\left(\theta_{\mathrm{d}} - \hat{\theta}\right) + K_{\mathrm{d},\theta}\left(\dot{\theta}_{\mathrm{d}} - \hat{\dot{\theta}}\right) + \ddot{\theta}_{\mathrm{d}} \tag{20b}$$

$$\nu_{\mathrm{r}} = \left(K_{\mathrm{p},r} + \frac{K_{\mathrm{i},r}}{s}\right)\left(r_{\mathrm{d}} - \hat{r}\right) \tag{20c}$$

with the desired quantities $_{\mathrm{d}}$ and controller gains K. A second-order reference model calculates the desired roll and pitch angles and derivatives similar to [21].

For the yaw axis, either a tracking of $\dot{\psi}$ in hover or $\boldsymbol{n}_{\mathrm{y}}$ in cruise flight is performed. The lateral load factor $\boldsymbol{n}_{\mathrm{y}}$ is controlled through the sideslip angle β by using the approximations $r \approx \dot{\beta}$ and

$$\Delta \boldsymbol{n}_{\mathrm{y}} \approx \frac{1}{g}\,\bar{q}\,S\,C_{\mathrm{Y},\beta}\,\Delta\beta \tag{21}$$

When commanding a roll angle ϕ_{d} in cruise flight, the aircraft performs a coordinated turn, i.e., $\boldsymbol{n}_{\mathrm{y}} = 0$. This can

either be achieved solely by the previously mentioned $\boldsymbol{n}_\mathrm{y}$-controller (and neglecting the $\dot{\psi}$ error) or by using a feed forward $\dot{\psi}$-command of the coordinated turn and converting it to a feed forward r-command. This is done per the following formulas

$$\dot{\psi}_\mathrm{d} \approx g \, \tan\phi \, \frac{\boldsymbol{v}_\mathrm{x}^C}{\left\|\boldsymbol{v}^C\right\|_2} \tag{22a}$$

$$r_\mathrm{d} \approx \dot{\psi}_\mathrm{d} \, \cos\phi \tag{22b}$$

with the gravitational acceleration g.

F. Flight Path Control

The flight path controller tracks the horizontal and vertical translational velocities in the control frame, v_x^C and v_z^C. The lateral velocity v_y^C is not controlled directly but via proxy commands in an outer loop by using translational rate command in hover mode and $\boldsymbol{n}_\mathrm{y}$ control in cruise flight. The velocities are controlled by a PI controller

$$\nu_{\boldsymbol{v}_\mathrm{x}^C} = \left(K_\mathrm{p} + \frac{K_\mathrm{i}}{s}\right)\left(\boldsymbol{v}_{\mathrm{x,d}}^C - \hat{\boldsymbol{v}}_\mathrm{x}^C\right) + \dot{\boldsymbol{v}}_{\mathrm{x,d}}^C \tag{23a}$$

$$\nu_{\boldsymbol{v}_\mathrm{x}^C} = \left(K_\mathrm{p} + \frac{K_\mathrm{i}}{s}\right)\left(\boldsymbol{v}_{\mathrm{z,d}}^C - \hat{\boldsymbol{v}}_\mathrm{z}^C\right) + \dot{\boldsymbol{v}}_{\mathrm{z,d}}^C \tag{23b}$$

The lateral virtual control input $\nu_{\boldsymbol{v}_\mathrm{y}^C}$ is set to the measured value $\hat{\boldsymbol{v}}_\mathrm{y}^C$. The gains in Eq. (23) depend on the longitudinal dynamics of the actuated plant and are heavily restricted by the bandwidth of the tilt actuator, as discussed in Section III.G. An alternative approach is to schedule the gains based on the current transformation state σ.

G. Pitch-supported tilting

As illustrated in Fig. 4, pitch attitude control can enhance the performance of tilt-wing longitudinal flight path control. To mitigate the performance limitations caused by low-bandwidth tilt actuators and saturation constraints (0° to 90°), we exploit the faster pitch dynamics, which have a similar influence on the dynamics, to compensate for tilt angle errors. This can be achieved through a strategy similar to Pseudo Control Hedging (PCH) [43].

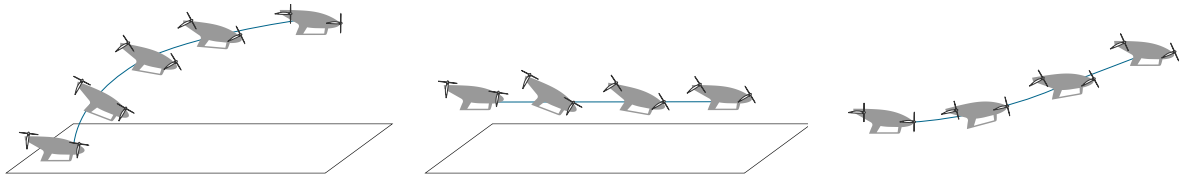

(a) Climbing transition maneuver (b) Horizontal motion during hover (c) Vertical motion during cruise

Fig. 4 Sketch of the pitch motion supporting the transition which is governed by slow tilt-wing dynamics.

The inversion law Eq. (13) calculates the optimal and unrestricted tilt angle commands $\delta_{w,1..2}^*$ and thrust commands

$T^*_{1..8}$ for the current state and force (and moment) demand τ_0. As a precaution, τ_0 is limited to $\tau_{0,\text{lim}}$ with $-8\bar{T} \leq \boldsymbol{f}^B_z \leq -8\underline{T}$ and $\underline{\boldsymbol{f}}^B_x \leq \boldsymbol{f}^B_x \leq 8\bar{T}$, where $\underline{T}$ and $\bar{T}$ denote the minimal and maximal thrust settings and $\underline{\boldsymbol{f}}^B_x$ the minimal force in x-direction that can be introduced by control inputs (i.e., mainly drag). A virtual tilt angle φ^* is introduced to represent the direction of the ideal and unrestricted thrust vector that realizes the demanded forces in the x- and z-direction. To stay close to the optimal command, the forces realized by the optimal commands are augmented by the τ_0-excess, i.e., the difference between the total demand τ_0 and the limited demand $\tau_{0,\text{lim}}$, yielding:

$$\varphi^* = \arctan \frac{\sum_{p=1}^{4} \sin \delta^*_{\text{w},p} T^*_p + \sum_{p=5}^{8} \sin \delta^*_{\text{w},p} T^*_p - \tau_{0,z} + \tau_{0,\text{lim},z}}{\sum_{p=1}^{4} \cos \delta^*_{\text{w},1} T^*_p + \sum_{p=5}^{8} \cos \delta^*_{\text{w},2} T^*_p + \tau_{0,x} - \tau_{0,\text{lim},x}} \tag{24}$$

The difference between φ^* and the actual thrust vector direction φ is the new pitch angle command, i.e., $\theta_{\text{com}} = \varphi^* - \varphi$.

IV. Simulation Results and Discussion

The capability and accuracy of the proposed inversion-based control approach is shown and analyzed in [27]. Subsequently, the focus is on the ability to transition between the different flight modes. Transition maneuvers are critical for tilt-wing aircraft operation, as they can lead to high angles of attack, potentially resulting in flow separation. The simulation model used is described in [28] and includes nonlinear effects on the propulsion, weight and balance, aerodynamics, and propulsion-aerodynamic couplings. Especially the nonlinear aerodynamic effects like flow separation are an inherent challenge and characteristic associated with tilt-wing aircraft transition maneuvers and must be considered in the control design and trajectory computation. However, by exploiting the slipstream effect and executing the transition rapidly, the effective angle of attack on each wing segment α^W_j can be reduced. Therefore, two common transition strategies from hover to cruise flight are investigated [4]: the *climbing* (or *outbound*) transition maneuver, i.e., smoothly transitioning from a vertical upward motion into a forward motion, and the *leveled* transition maneuver. The trajectory and characteristic of the transition maneuvers are visualized by their simulation results in Fig. 5.

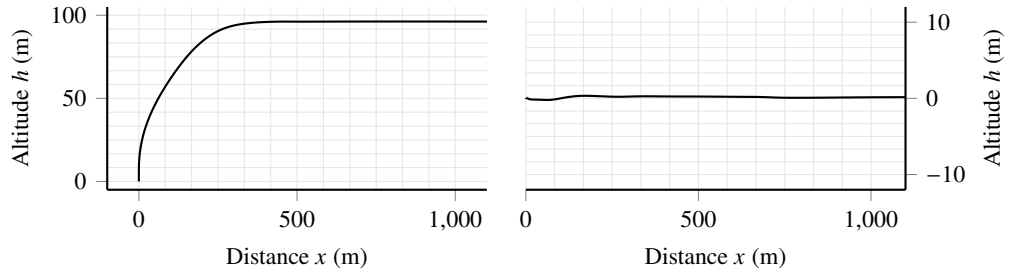

(a) Climbing transition trajectory (b) Leveled (or forward) transition trajectory

Fig. 5 Simulation results of the flight trajectories for the different transition maneuvers

In all plots, the solid line (——) represents measured signals and the dashed line (- - -) the reference commands.

A. Climbing Transition

For tilt-wing aircraft, it is advisable to transition in such a way that the wing (segments) do not stall. This makes the climbing transition a suitable maneuver as it roughly aligns the wings with the airflow (see [4]). In this scenario, the aircraft starts in a trimmed hover flight and receives a horizontal velocity command $\boldsymbol{v}_{\mathrm{x}}^{C} = 50\ \frac{\mathrm{m}}{\mathrm{s}}$ at 10 s after receiving an initial vertical velocity ramp up to $\boldsymbol{v}_{\mathrm{z}}^{C} = -8\ \frac{\mathrm{m}}{\mathrm{s}}$. When reaching the commanded velocity, the aircraft enters a trimmed cruise flight. The flight trajectory then results in a relatively smooth climbing transition curve. The results of the simulation are shown in Figure 6.

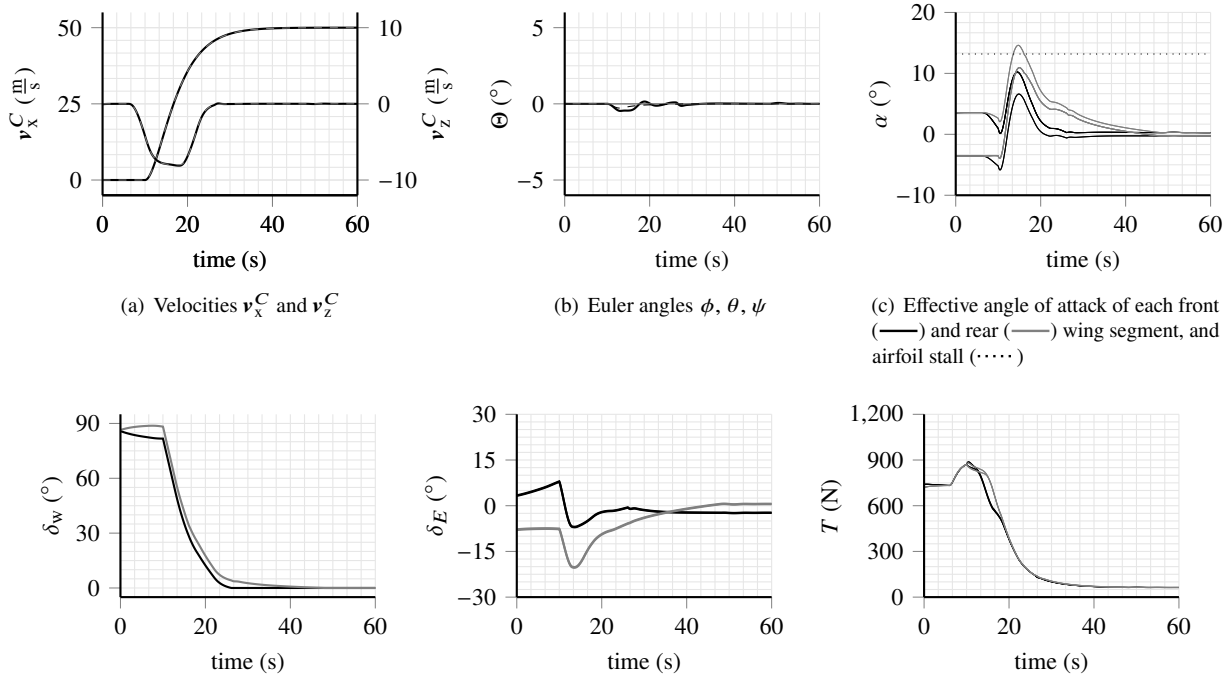

(a) Velocities $\boldsymbol{v}_{\mathrm{x}}^{C}$ and $\boldsymbol{v}_{\mathrm{z}}^{C}$

(b) Euler angles ϕ, θ, ψ

(c) Effective angle of attack of each front (——) and rear (——) wing segment, and airfoil stall (· · · · ·)

(d) Tilt angles δ_w of front (——) and rear (——) wing

(e) Elevon deflections δ_e at front (——) and rear (——) wing

(f) Thrust T of front (——) and rear (——) propellers

Fig. 6 Climbing transition maneuver.

As discussed in [4], the climbing transition is a strategy that helps to avoid flow separation during transition. Thus, the climbing transition is a suitable starting maneuver to demonstrate the controller's capability for global inversion, excluding post-stall regions. The results indicate that the proposed control law can smoothly perform a climbing transition. Furthermore, it does not utilize excessive or sharp control commands. Moreover, flow separation is effectively mitigated as the aircraft mainly remains below the critical angle of attack of the plain airfoil. Solely the two inner segments of the rear wing briefly reach the critical angle of attack due to the swirl effect of the propellers. However, this stall avoidance is achieved by the selection of the reference signal, rather than being an inherent characteristic of the control law. The controller emulates global inversion capabilities by providing local solutions throughout the flight envelope. This is suggested by the results, as the controller effectively decouples and tracks the velocities and attitudes

throughout the maneuver, during which the aircraft traverses a large part of the flight envelope. It is also noteworthy that both tilt angles drift apart before the maneuver is initiated. This effect arises from the redistribution of the control effectors, which minimizes the control allocation objective. This phenomenon occurs when the trimmed starting point is not optimal in terms of the control allocation objective.

B. Leveled or Forward Transition

While the climbing transition maneuver is a common strategy for reaching cruise flight with a tilt-wing aircraft, an alternative and more intuitive transition strategy is the leveled transition, where the aircraft maintains its current altitude and only accelerates forward. However, this causes the wing to approach or enter the stall region of most airfoils. Nevertheless, depending on design and strategy, the leveled transition is a valid option for (tandem) tilt-wing aircraft transition (see [4]). The setup is similar to the climbing transition, but this time the current flight level is maintained, i.e., $\boldsymbol{v}_z^C = 0\,\frac{\mathrm{m}}{\mathrm{s}}$. Figure 7 shows the results of this experiment.

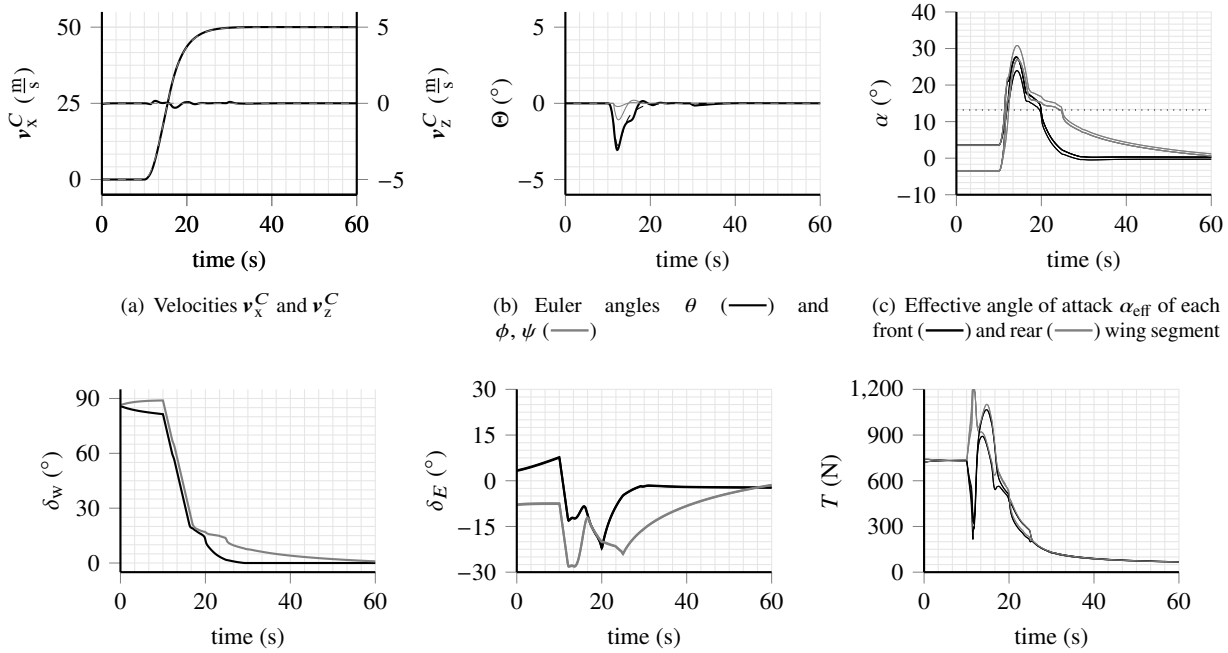

(a) Velocities $\boldsymbol{v}_x^C$ and $\boldsymbol{v}_z^C$

(b) Euler angles θ (——) and ϕ, ψ (——)

(c) Effective angle of attack α_{eff} of each front (——) and rear (——) wing segment

(d) Tilt angles δ_w of front (——) and rear (——) wing

(e) Elevon deflections δ_e at front (——) and rear (——)

(f) Thrust T of front (——) and rear (——) propellers

Fig. 7 Leveled transition maneuver.

The results depicted in Fig. 7 demonstrate that the transition can be successfully completed. The velocity command is tracked smoothly and the altitude is kept within a sufficiently small boundary. Compared to the climbing transition, the angle of attack is increased by up to 15°, effectively stalling the wing segment. An effect of this can not only be seen in the v_z^C trend, but more noticeable in the thrust trend. Since the flow separation results in an increased pitching moment, differential thrust between the front and rear wings is required to compensate for the moment.

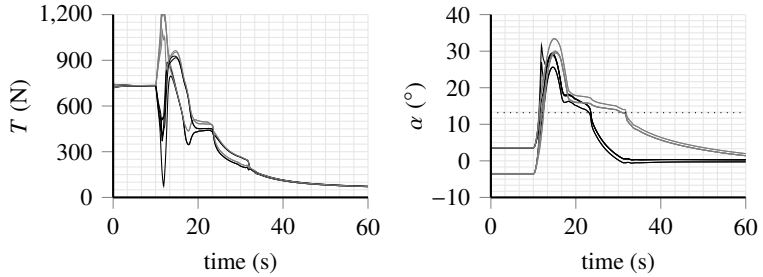

Fig. 8 Thrust of front (——) and rear (——) propellers and angle of attack of each front (——) and rear (——) wing segment in a leveled transition maneuver without pitch-supported tilting.

The effect of the *pitch-supported tilting* can be seen in the pitch angle trend in Fig. 7b, which follows its command smoothly. There is also a reduction in the thrust difference and the angle of attack compared to the non-pitching case shown in Fig. 8.

V. Conclusion

Transformational vertical take-off and landing (VTOL) aircraft, including tilt-wing electric VTOLs (eVTOLs), are capable of seamlessly transitioning between hover and forward flight. However, their complex mechanics, aerodynamic interactions, and changing dynamics throughout the flight phases present significant challenges for control design. This study proposes a unified control approach using hybrid nonlinear dynamic inversion (hybrid NDI) combined with optimization-based control allocation and applies it to a tandem tilt-wing eVTOL. The angular rate and velocity inversion law is cascaded with a parallel attitude and flight path controller to address the multifaceted flight control task and utilize the available degrees of freedom from the aircraft configuration. This leads to a single control law that can effectively handle all flight phases of the vehicle, including the transition. The implementation is demonstrated and tested using a strip theory-based 6-DoF flight dynamics model. The results confirm the presumed properties, indicating that the control law can invert the tilt-wing dynamics over the flight envelope, allowing the seamless execution of different transition maneuvers. The results of this study lay the foundation for achieving unified multi-phase tandem tilt-wing flight.

References

[1] Bacchini, A., and Cestino, E., "Electric VTOL Configurations Comparison," *Aerospace*, Vol. 6, No. 3, 2019. https://doi.org/10.3390/aerospace6030026.

[2] Cook, J., "A Strip Theory Approach to Dynamic Modeling of eVTOL Aircraft," *AIAA SCITECH 2021 Forum*, 2021. https://doi.org/10.2514/6.2021-1720, AIAA Paper 2021-1720.

[3] Simmons, B. M., and Murphy, P. C., "Aero-Propulsive Modeling for Tilt-Wing, Distributed Propulsion Aircraft Using Wind Tunnel Data," *Journal of Aircraft*, Vol. 59, No. 5, 2022, pp. 1162–1178. https://doi.org/10.2514/1.C036351.

[4] May, M., Milz, D., Armanini, S., and Looye, G., "Transition Strategies for Tilt-Wing Aircraft," *Journal of Guidance, Control, and Dynamics*, Vol. 48, No. 10, 2025, pp. 2326–2337. https://doi.org/10.2514/1.G008257.

[5] Sullivan, T., "The Canadair CL-84 tilt wing design," *Aircraft Design, Systems, and Operations Meeting*, 1993. https://doi.org/10.2514/6.1993-3939.

[6] Droandi, G., Syal, M., and Bower, G., "Tiltwing Multi-Rotor Aerodynamic Modeling in Hover, Transition and Cruise Flight Conditions," *AHS International 74th Annual Forum & Technology*, 2018.

[7] North, D. D., Busan, R. C., and Howland, G., "Design and Fabrication of the LA-8 Distributed Electric Propulsion VTOL Testbed," *AIAA SCITECH 2021 Forum*, 2021. https://doi.org/10.2514/6.2021-1188, AIAA Paper 2021-1188.

[8] Panish, L., Nicholls, C., and Bacic, M., "Nonlinear Dynamic Inversion Flight Control of a Tiltwing VTOL Aircraft," *AIAA SCITECH 2023 Forum*, AIAA, 2023. https://doi.org/10.2514/6.2023-1910, AIAA Paper 2023-1910.

[9] Holsten, J., Ostermann, T., Dobrev, Y., and Moormann, D., "Model validation of a tiltwing UAV in transition phase applying windtunnel investigations," *Congress of the International Council of the Aeronautical Sciences*, Vol. 28, International Council of the Aeronautical Sciences Bonn, Germany, 2012, pp. 1–10.

[10] Cetinsoy, E., Dikyar, S., Hancer, C., Oner, K. T., Sirimoglu, E., Unel, M., and Aksit, M. F., "Design and construction of a novel quad tilt-wing UAV," *Mechatronics*, Vol. 22, No. 6, 2012, pp. 723–745. https://doi.org/10.1016/j.mechatronics.2012.03.003.

[11] Raab, S. A., Zhang, J., Bhardwaj, P., and Holzapfel, F., "Proposal of a Unified Control Strategy for Vertical Take-off and Landing Transition Aircraft Configurations," *2018 Applied Aerodynamics Conference*, AIAA, 2018. https://doi.org/10.2514/6.2018-3478, AIAA Paper 2018-3478.

[12] Panish, L., and Bacic, M., "A Generalized Full-Envelope Outer-Loop Feedback Linearization Control Strategy for Transition VTOL Aircraft," *AIAA AVIATION 2023 Forum*, AIAA, 2023. https://doi.org/10.2514/6.2023-4511, AIAA Paper 2023-4511.

[13] Liu, Z., He, Y., Yang, L., and Han, J., "Control techniques of tilt rotor unmanned aerial vehicle systems: A review," *Chinese Journal of Aeronautics*, Vol. 30, No. 1, 2017, pp. 135–148. https://doi.org/10.1016/j.cja.2016.11.001.

[14] Hartmann, P., Meyer, C., and Moormann, D., "Unified Velocity Control and Flight State Transition of Unmanned Tilt-Wing Aircraft," *Journal of Guidance, Control, and Dynamics*, Vol. 40, No. 6, 2017, pp. 1348–1359. https://doi.org/10.2514/1.g002168.

[15] Dickeson, J. J., Miles, D., Cifdaloz, O., Wells, V. L., and Rodriguez, A. A., "Robust LPV H_∞ gain-scheduled hover-to-cruise conversion for a tilt-wing rotorcraft in the presence of CG variations," *2007 46th IEEE Conference on Decision and Control*, IEEE, 2007. https://doi.org/10.1109/cdc.2007.4435028.

[16] Cook, J., and Gregory, I., "A Robust Uniform Control Approach for VTOL Aircraft," *Vertical Flight Society – 2021 Autonomous VTOL Technical Meeting and Electric VTOL Symposium*, 2021.

[17] Daud Filho, A., and Belo, E., "A tilt-wing VTOL UAV configuration: Flight dynamics modelling and transition control simulation," *The Aeronautical Journal*, Vol. 128, No. 1319, 2023, pp. 152–177. https://doi.org/10.1017/aer.2023.34.

[18] Sobiesiak, L. A., Fortier-Topping, H., Beaudette, D., Bolduc-Teasdale, F., Lafontaine, J. D., Nagaty, A., Neveu, D., and Rancourt, D., "Modelling and Control of Transition Flight of an eVTOL Tandem Tilt-Wing Aircraft," *8th European Conference for Aeronautics and Aerospace Sciences (EUCASS)*, Proceedings of the 8th European Conference for Aeronautics and Space Sciences. Madrid, Spain, 1-4 july 2019, 2019. https://doi.org/10.13009/EUCASS2019-137.

[19] Autenrieb, J., Shin, H.-S., and Bacic, M., "Development of a Neural Network-based Adaptive Nonlinear Dynamic Inversion Controller for a Tilt-wing VTOL Aircraft," *2019 Workshop on Research, Education and Development of Unmanned Aerial Systems (RED UAS)*, 2019, pp. 44–52. https://doi.org/10.1109/REDUAS47371.2019.8999700.

[20] Axten, R. M., Khamvilai, T., and Johnson, E. N., "VTOL Freewing Design and Adaptive Controller Development," *AIAA SCITECH 2023 Forum*, 2023. https://doi.org/10.2514/6.2023-0401, AIAA Paper 2023-0401.

[21] Milz, D., and Looye, G., "Tilt-Wing Control Design for a Unified Control Concept," *AIAA SCITECH 2022 Forum*, 2022. https://doi.org/10.2514/6.2022-1084, AIAA Paper 2022-1084.

[22] Surmann, D., and Myschik, S., "Gain Design of an INDI-based Controller for a Conceptual eVTOL in a Nonlinear Simulation Environment," *AIAA SCITECH 2023 Forum*, 2023. https://doi.org/10.2514/6.2023-1250, AIAA Paper 2023-1250.

[23] Di Francesco, G., and Mattei, M., "Modeling and Incremental Nonlinear Dynamic Inversion Control of a Novel Unmanned Tiltrotor," *Journal of Aircraft*, Vol. 53, No. 1, 2016, pp. 73–86. https://doi.org/10.2514/1.C033183.

[24] Lombaerts, T., Kaneshige, J., Schuet, S., Aponso, B. L., Shish, K. H., and Hardy, G., "Dynamic Inversion based Full Envelope Flight Control for an eVTOL Vehicle using a Unified Framework," *AIAA SCITECH 2020 Forum*, 2020. https://doi.org/10.2514/6.2020-1619, AIAA Paper 2020-1619.

[25] Binz, F., Islam, T., and Moormann, D., "Attitude control of tiltwing aircraft using a wing-fixed coordinate system and incremental nonlinear dynamic inversion," *International Journal of Micro Air Vehicles*, Vol. 11, 2019, p. 175682931986137. https://doi.org/10.1177/1756829319861370.

[26] Liu, Z., Guo, J., Li, M., Tang, S., and Wang, X., "VTOL UAV Transition Maneuver Using Incremental Nonlinear Dynamic Inversion," *International Journal of Aerospace Engineering*, Vol. 2018, 2018, pp. 1–19. https://doi.org/10.1155/2018/6315856.

[27] Milz, D., May, M., and Looye, G., "Dynamic Inversion-Based Control Concept for Transformational Tilt-Wing eVTOLs," *AIAA SCITECH 2024 Forum*, AIAA, 2024. https://doi.org/10.2514/6.2024-1290, AIAA Paper 2024-1290.

[28] May, M. S., Milz, D., and Looye, G., "Semi-Empirical Aerodynamic Modeling Approach for Tandem Tilt-Wing eVTOL Control Design Applications," *AIAA SCITECH 2023 Forum*, 2023. https://doi.org/10.2514/6.2023-1529, AIAA Paper 2023-1529.

[29] Kumtepe, Y., Pollack, T., and van Kampen, E.-J., "Flight Control Law Design using Hybrid Incremental Nonlinear Dynamic Inversion," *AIAA SCITECH 2022 Forum*, AIAA, 2022. https://doi.org/10.2514/6.2022-1597, AIAA Paper 2022-1597.

[30] Milz, D., May, M., and Looye, G., "Flight Testing Air Data Sensor Failure Handling with Hybrid Nonlinear Dynamic Inversion," *Proceedings of the 2024 CEAS EuroGNC conference*, 2024.

[31] May, M., Milz, D., Armanini, S. F., and Looye, G., "Impact of Failure on the Tilt-Wing eVTOL Backward Transition," *Journal of Aircraft*, Vol. 0, No. 0, 0, pp. 1–13. https://doi.org/10.2514/1.C038391.

[32] Öner, K. T., Çetinsoy, E., Sirimoğlu, E., Hançer, C., Ünel, M., Akşit, M. F., Gülez, K., and Kandemir, I., "Mathematical modeling and vertical flight control of a tilt-wing UAV," *Turkish Journal of Electrical Engineering & Computer Sciences*, Vol. 20, No. 1, 2012, pp. 149–157.

[33] Sieberling, S., Chu, Q. P., and Mulder, J. A., "Robust Flight Control Using Incremental Nonlinear Dynamic Inversion and Angular Acceleration Prediction," *Journal of Guidance, Control, and Dynamics*, Vol. 33, No. 6, 2010, pp. 1732–1742. https://doi.org/10.2514/1.49978.

[34] Kier, T. M., Müller, R., and Looye, G., "Analysis of Automatic Control Function Effects on Vertical Tail Plane Critical Load Conditions," *AIAA SCITECH 2020 Forum*, AIAA, 2020. https://doi.org/10.2514/6.2020-1621, AIAA Paper 2020-1621.

[35] Steffensen, R., Steinert, A., and Smeur, E. J. J., "Non-Linear Dynamic Inversion with Actuator Dynamics: an Incremental Control Perspective," *Journal of Guidance, Control, and Dynamics*, Vol. 46, No. 4, 2023, pp. 709–717. https://doi.org/10.2514/1.G007079.

[36] Autenrieb, J., and Shin, H.-S., "Complementary Filter-Based Incremental Nonlinear Model Following Control Design for a Tilt-Wing UAV," *International Journal of Robust and Nonlinear Control*, Vol. 35, No. 4, 2025, pp. 1596–1615. https://doi.org/https://doi.org/10.1002/rnc.7743, URL https://onlinelibrary.wiley.com/doi/abs/10.1002/rnc.7743.

[37] Jiali, Y., and Jihong, Z., "An angular acceleration estimation method based on the complementary filter theory," *2016 IEEE International Instrumentation and Measurement Technology Conference Proceedings*, 2016, pp. 1–6. https://doi.org/10.1109/I2MTC.2016.7520548.

[38] Wang, X., van Kampen, E.-J., Chu, Q., and Lu, P., "Stability Analysis for Incremental Nonlinear Dynamic Inversion Control," *Journal of Guidance, Control, and Dynamics*, Vol. 42, No. 5, 2019, pp. 1116–1129. https://doi.org/10.2514/1.g003791.

[39] Pollack, T., and van Kampen, E.-J., "Multi-objective Design and Performance Analysis of Incremental Control Allocation-based Flight Control Laws," *AIAA SCITECH 2023 Forum*, 2023. https://doi.org/10.2514/6.2023-1249, AIAA Paper 2023-1249.

[40] Pfeifle, O., and Fichter, W., "Minimum Power Control Allocation for Incremental Control of Over-Actuated Transition Aircraft," *Journal of Guidance, Control, and Dynamics*, Vol. 46, No. 2, 2023, pp. 286–300. https://doi.org/10.2514/1.G006929.

[41] Enns, D., Bugajski, D., Hendrick, R., and Stein, G., "Dynamic inversion: an evolving methodology for flight control design," *International Journal of Control*, Vol. 59, No. 1, 1994, pp. 71–91. https://doi.org/10.1080/00207179408923070.

[42] Spivak, M., *Calculus On Manifolds: A Modern Approach To Classical Theorems Of Advanced Calculus*, 1st ed., CRC Press, 1965. https://doi.org/10.1201/9780429501906.

[43] Johnson, E. N., and Calise, A. J., "Pseudo-control hedging: A new method for adaptive control," *Advances in Navigation Guidance and Control Technology Workshop*, Alabama, USA Alabama, USA, 2000, pp. 1–2.